ACS APPLIED MATERIALS & INTERFACES

Research Article

www.acsami.org

New Physical Deposition Approach for Low Cost Inorganic Hole Transport Layer in Normal Architecture of Durable Perovskite Solar Cells

Bahram Abdollahi Nejand,[†] Vahid Ahmadi,[*,‡] and Hamid Reza Shahverdi[†]

[†]Nanomaterials Group, Department of Materials Engineering, Tarbiat Modares University, 14115-194 Tehran, Iran

[‡]School of Electrical and Computer Engineering, Tarbiat Modares University, 14115-194 Tehran, Iran

Supporting Information

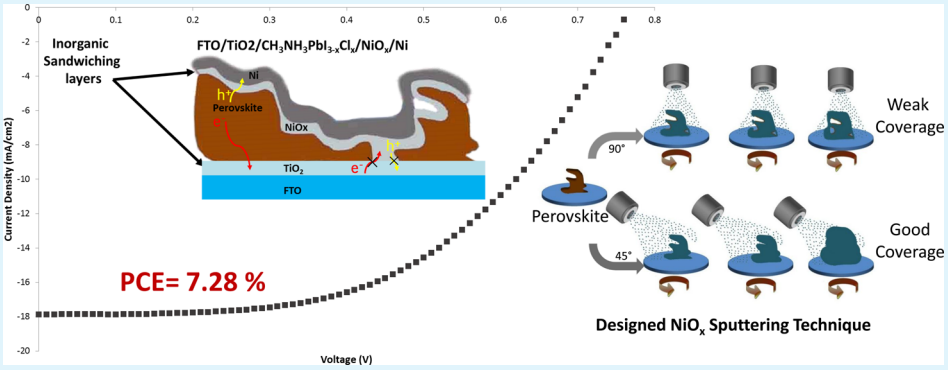

ABSTRACT: In this work we reported sputter deposited NiO_x/Ni double layer as an HTM/contact couple in normal architecture of perovskite solar cell. A perovskite solar cell that is durable for more than 60 days was achieved, with increasing efficiency from 1.3% to 7.28% within 6 days. Moreover, low temperature direct deposition of NiO_x layer on perovskite layer was introduced as a potential hole transport material for an efficient cost-effective solar cell applicable for various morphologies of perovskite layers, even for perovskite layers containing pinholes, which is a notable challenge in perovskite solar cells. The angular deposition of NiO_x layers by dc reactive magnetron sputtering showed uniform and crack-free coverage of the perovskite layer with no negative impact on perovskite structure that is suitable for nickel back contact layer, surface shielding against moisture, and mechanical damages. Replacing the expensive complex materials in previous perovskite solar cells with low cost available materials introduces cost-effective scalable perovskite solar cells.

KEYWORDS: *inorganic hole transport material, planar perovskite solar cell, sputter deposited NiO_x, durable, low cost and temperature*

1. INTRODUCTION

As a potential light absorber, organometal trihalide perovskite (OTP) structures explore a wide range of highly efficient solar cells. During the past years, many studies have been conducted to enhance the efficiency, durability, and cost-effectiveness of the perovskite solar cells (PSCs).[1−4] The OTP is an ideal photovoltaic material that exhibits an almost 1.5 eV direct optical band gap and allows exciton bonding energy and long diffusion length (∼1 μm) and a broad range of light absorption covering the visible to near-infrared spectrum (800 nm) with high extinction coefficient (∼10^4 cm $^{-1}$ at 550 nm).[5−7] Choosing an appropriate electron transport material (ETM) and hole transport material (HTM) for extracting electron and hole, respectively, from OTP absorber has a high impact on PSC efficiency. By now, a certified 20.1% power conversion efficiency[8] was reported while the previous certified report was 17.9%.[9] Nevertheless, using expensive materials such as 2,29,7,79-tetrakis(*N*,*N*-di-*p*-methoxyphenylamino)-9,99-spirobifluorene (spiro-OMeTAD),[4,10,11] poly(3,4-ethylenedioxythiophene), (PEDOT:PSS),[12−14] poly(3-hexylthiophene) (P3HT), poly[bis(4-phenyl) (2,4,6-trimethylphenyl)-amine] (PTAA), and carbon nanotubes (CNTs)[15,16] as HTM, [6,6]-phenyl-C61-butyric acid methyl ester (PCBM)[12,17,18] as ETM, and also noble metals (Au, Ag, Pt) as counter electrodes impose a high cost for fabrication of PSCs. In some attempts, scientists achieved valuable results in decreasing the cost of PSCs fabrication by substituting the HTM and noble metals counter electrode by graphite and carbon electrodes.[19,20] To reach a low cost PCS, in some works, in addition to TiO_2,[21,22] ZnO,[10,23] and Al_2O_3 (as an inert wide band gap scaffold structure),[24,25] as the low cost ETMs, cheaper inorganic materials such as CuI[26] and CuSCN[27] as HTMs are also reported. In this regard, graphite and carbon electrodes[19,20] are employed as hole conductor free PCSs. Furthermore, in some inverted structures,

Received: June 26, 2015
Accepted: September 18, 2015
Published: September 24, 2015

DOI: 10.1021/acsami.5b05477
ACS Appl. Mater. Interfaces 2015, 7, 21807−21818

NiO and NiO_x are used as a potential HTM instead of spiro-MeOTAD.[18,28] However, it is worth mentioning that, in these structures, PCBM is used as an ETM, which is considered as an expensive material. Replacing the organic HTM with inorganic materials improves the device stability and provides versatile choices for materials selection and device design. Besides, in some interesting attempts, using nickel as a cathode contact on the spiro-MeOTAD showed a 10.4% power conversion efficiency. Thus, using this material is regarded as an appropriate candidate for the gold contact replacement with the reported 11.6% power conversion efficiency.[29]

By removing the mesoscopic layer, planar heterojunction device architectures are gradually attracting more attention, as they simplify device preparation and reduce material cost. Many reported planner PSCs such as TiO_2/perovskite/spiro-MeOTAD,[30,31] ZnO/perovskite/spiro-MeOTAD,[8,32] and PEDOT:PSS/perovskite/C_{60}[12,17] showed low cost fabrication with optimum 15.7% efficiency, which competes with that of mesoscopic PSCs. In a majority of works, except those conducted on printable graphite counter PSCs (which involve two to three step high temperature sintering processes needing considerable time and cost), using one of the high cost materials as ETM (such as PCBM) or HTM (such as spiro-MeOTAD, P3HT, and PTAA) is common. On the basis of the interesting properties of NiO_x such as optical transparency, chemical stability, good conductivity of holes, tunable work function from 5.0 to 5.6 eV, and low cost, we chose it as a potential electrode interlayer in inorganic sandwiched PSCs. As the perovskite layers are highly sensitive to some solvents and deposition processes, to complete the device in both direct and inverted structures, the methods for uniform perovskite surface coverage are limited to some polymeric based materials. Moreover, there is no report in physical deposition on the perovskite top layer due to some limitations in surface coverage, generated heat, and structure infiltration. In addition, using metal oxides as both n-type and p-type materials for PSCs is a future vision and has appeal because of their robust behavior, long-term durability, low cost, and, above all, environment and market friendly characteristics. In this work, we successfully replaced the high cost HTMs and ETMs previously reported in PSC works in PSCs using compact rutile TiO_2 as an ETM and NiO_x/Ni as a HTM/noble metal contact. Since filling the nonflat structure of perovskite prepared by common two-step methods and some ununiformed one-step methods is impossible using normal sputtering methods, in this report we achieved a highly durable PSC by controlling the engineered NiO_x sputtered layer on $CH_3NH_3Pb_{3-x}Cl_3$ perovskite layer.

Sputtering is among the interesting methods in deposition of uniform, dense, and pinhole-free semiconductors and metal layers and is an appropriate method for deposition of low roughness surfaces. Despite all remarkable properties of deposited layers by the normal sputtering method, the low surface coverage of rough surfaces is one of the noticed shortcomings in the use of this method in fabrication of PSCs. Hence, engineering the deposition technology in sputtered layers for achieving satisfactory perovskite layer coverage may fulfill both low cost and scale-up possibility aspects in PSC fabrication. Besides, generated heat during the deposition and accelerated atoms within the sputtering method can affect the perovskite layer and, as a result, the cell performance. Therefore, designing a comprehensive and precise technique pointing to the effective parameters in deposition of both NiO_x and Ni layer on perovskite layer might alleviate some problems involved in inorganic sandwiched PSCs and allow its industrial feasibility.

In this work, we successfully deposited a robust and uniform NiO_x thin film on a perovskite layer for extracting the generated hole from the perovskite layer and subsequently a nickel layer as a contact with a work function state very close to that of gold and NiO_x HOMO. Sputter deposited NiO_x as an inorganic HTM on perovskite layer in normal architectures has not been reported so far.

2. EXPERIMENTAL DETAILS

2.1. Preparing Compact Layer. FTO-coated glass substrates were patterned by Zn powder and 2 M HCl etching solution. The patterned FTO substrates were cleaned by soap−deionized water solution, followed by ultrasonication at 50 °C deionized water, ethanol, and isopropanol and then were subjected to an O_3/ultraviolet treatment for 20 min. After cleaning the substrates, the back side and contact part of FTO side were masked by pieces of transparent adhesive tape. A rutile TiO_2 compact layer was prepared on the basis of the previously reported procedure.[31] In brief, the masked FTO layers were immersed into 200 mM $TiCl_4$ in DI water solution placed in a sealed container and kept in an oven at 70 °C for 1 h. After gently washing the deposited FTO substrates with water and ethanol for 1 min, the tape masks were removed and dried at 100 °C in air for an hour. After drying, the contact part of the FTO side was masked again by pieces of tranparent adhesive tape to be prepared for future perovskite deposition.

2.2. Synthesis of CH_3NH_3I. The CH_3NH_3I was synthesized by reacting 24 mL of CH_3NH_2 and 10 mL of HI in a 250 mL round-bottom flask at 0 °C for 2 h with stirring. The precipitate was collected using a rotary evaporator through careful removal of the solvents at 50 °C. The as-obtained product was redissolved in 100 mL of absolute ethanol and precipitated with addition of 300 mL of diethyl ether, and this procedure was repeated thrice. The final CH_3NH_3I was collected and dried at 60 °C in a vacuum oven for 24 h.

2.3. Deposition of Perovskite Layer. Deposition of the perovskite layer on thin rutile TiO_2 compact layers was done at room temperature and air atmosphere with 20% moisture content. For the perovskite layer, a 1:3 ratio of $PbCl_2$:CH_3NH_3I with the concentrations 203 and 350 mg were mixed in 1 mL of DMF, respectively. The mixture solution was stirred at room temperature overnight and spin-coated on rutile TiO_2 compact layers at 2000 rpm for 30 s, and then annealed at 100 °C for 45 min.

2.4. NiO_x/Ni Sputtering Layer. For deposition of NiO_x electron barrier layer on the as-prepared perovskite layer, dc reactive magnetron sputtering of industrial metallic nickel target (99.97%) was used. NiO_x deposition was carried out in 3 mTorr oxygen atmosphere (99.9995%), 12 cm distance of nickel target, and 80 W power. To inhibit temperature rising during the sputtering, we adjusted the distance between target and substrates, besides using noncontinuous deposition with 15 min deposition and 10 min delay between any sequences. Maximum substrate temperature was 95 °C. For good coverage of the perovskite surface by NiO_x, the rotating substrate holder was used. Thickness measurement was done by piezoelectric thickness measurement apparatus (SQM-242 codeposition control and software, Sigma Instrument) for various 10, 20, 30, 40, and 50 nm thicknesses of NiO_x layers. A NiO_x layer was deposited on a whole perovskite layer, except the masked

DOI: 10.1021/acsami.5b05477
ACS Appl. Mater. Interfaces 2015, 7, 21807−21818

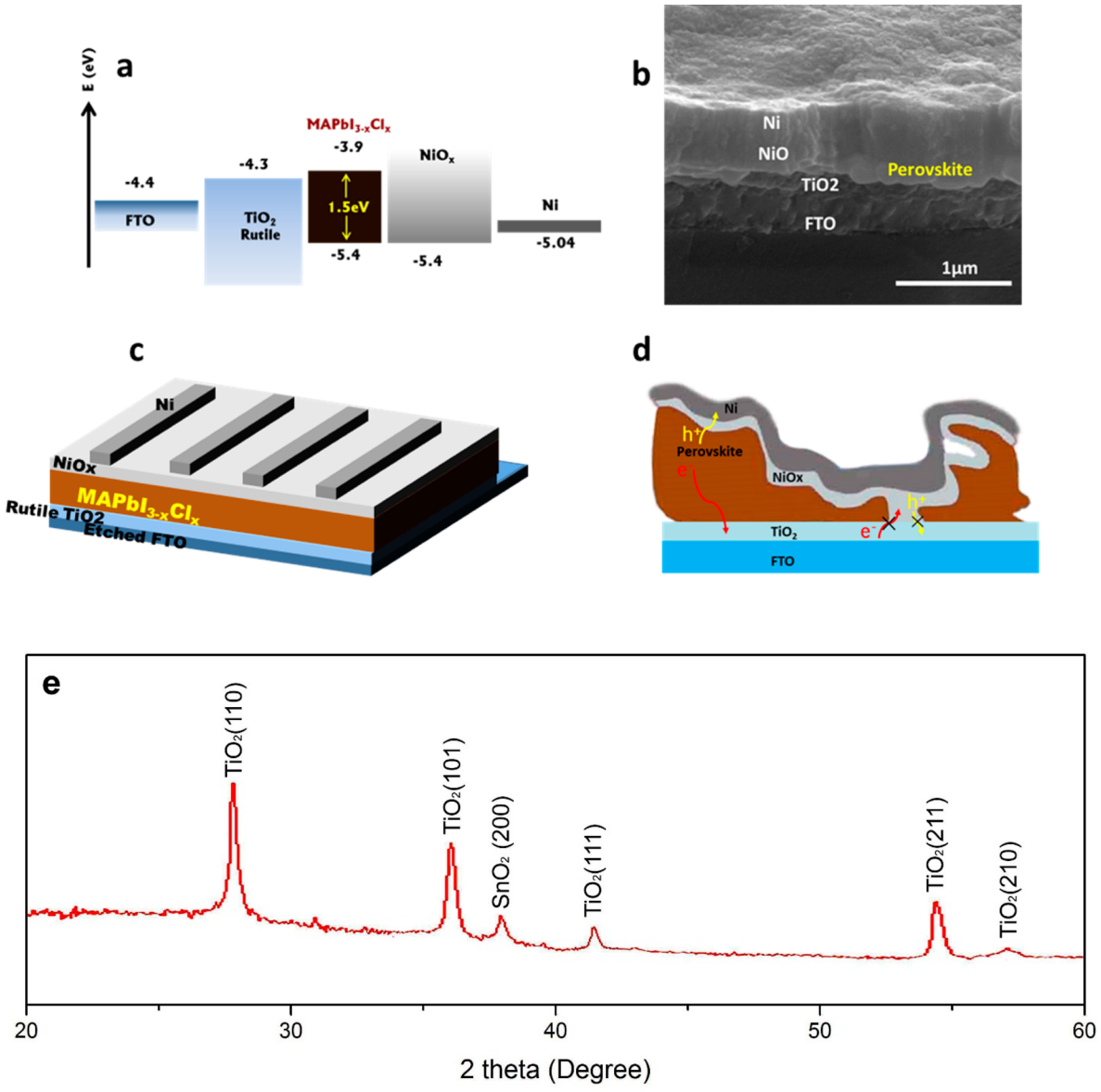

Figure 1. (a) Schematic energy level diagrams of the FTO/TiO_2/$CH_3NH_3PbI_{3-x}Cl_x$/NiO_x. (b) Cross sectional FE-SEM image of FTO/TiO_2/$CH_3NH_3PbI_{3-x}Cl_x$/NiO_x. (c) Schematic structure of the prepared device. (d) Charge generation and transport mechanism of the inorganic sandwiched perovskite solar cell. (e) Grazing incident XRD pattern of rutile TiO_2 compact layer grown on FTO substrate.

contact part of FTO in a rotating 45° tilted substrate for having a uniform coverage on rough surface of the perovskite layer. For nickel contact, after NiO_x deposition, a 0.1 cm^2 active area shadow mask with a nonsubstrate rotating and 90° deposition angle was used. Nickel contact deposition was carried out at 3 mTorr deposition pressure of argon atmosphere (99.9995%), industrial nickel target (99.97%), and 75 W dc magnetron power. The nickel contact thickness was 250 nm. Monitoring the deposition temperature on the substrate surface indicates that the cell temperature did not exceed 100 °C.

2.5. Prepared Device by Spiro-OMeTAD/Ag. Right after the annealed perovskite layers were cooled to room temperature, the spiro-OMeTAD based hole transporting layer [72 mg spiro-OMeTAD, 17.5 μL lithium-bis-(trifluoromethanesulfonyl)imide (Li-TFSI) solution (520 mg Li-TFSI in 1 mL of acetonitrile), and 26.6 mg of 4-*tert*-butylpyridine all dissolved in 1 mL chlorobenzene] was deposited by spin-coating at 2000 rpm for 30 s. With the deposited spiro-OMeTAD kept in a desiccator for 12 h, the thin 150 nm silver contact was deposited on the spiro-OMeTAD by a thin stainless steel shadow mask to create a 0.1 cm^2 active area.

2.6. Thin Film and Device Characterization. To study the microstructure and morphology of the deposited films, field emission scanning electron microscopy (FE-SEM, S4160 Hitachi) and atomic force microscopy (AFM, Veeco PCResearch) were used. The phase structure and crystal size of films were also investigated by X-ray diffraction (XRD, Philips Expert-MPD). XRD was performed in the θ–2θ mode using Cu Kα with wavelength of 1.5439 Å radiation. All the XRD experiments were performed at grazing incident angle of 2°. The optical characteristics of deposited films were analyzed by UV–vis spectroscopy using the wavelength range 190–1000 nm. The photocurrent–voltage (I–V) characteristics of solar cells were measured under one sun (AM1.5G, 100 mW/cm^2) illumination with a solar simulator (Sharif solar simulator). The

DOI: 10.1021/acsami.5b05477
ACS Appl. Mater. Interfaces 2015, 7, 21807–21818

four-point collinear probe method (Signatone) was used to measure the sheet resistivity. Steady-state PL measurements were acquired using a Varian Cary Eclipse fluorescence spectrometer.

3. RESULTS AND DISCUSSION

Figure 1a shows the energy level diagram of the FTO/TiO_2/$CH_3NH_3PbI_{3-x}Cl_x$/NiO_x/Ni device, containing two inorganic electron (TiO_2) and hole (NiO_x) extraction sandwich layers for PSC. As shown in the band diagrams, generated electrons can easily transfer to the TiO_2 layer because of high electron affinity of TiO_2 in the interface of TiO_2 and the perovskite layer, and the generated hole can preferably diffuse into the NiO_x layer considering the 5.4 eV band level diagram adjustment for both perovskite and NiO_x layers. Figure 1b illustrates field emission scanning electron microscopy of inorganic sandwiched PSCs with total thickness being less than 1000 nm. In the present study, we employed a compact layer of TiO_2 rutile structure grown by a simple method of chemical bath deposition at the low temperature of 70 °C, which resulted in a strong charge extraction on the rutile TiO_2 layer as compared to that of anatase structure.[31] After deposition of a perovskite layer on low roughness surface of TiO_2 through one-step spin coating of CH_3NH_3I and $PbCl_2$ solution, a well-covered and uniform thin NiO_x film using rotational 45° substrate reactive magnetron sputtering was deposited on rough perovskite layer. By completing the NiO_x deposition, a 250 nm nickel layer was deposited through a 0.1 cm^2 shadow mask creating active area. Figure 1c shows the order of layers in the FTO/TiO_2/$CH_3NH_3PbI_{3-x}Cl_x$/NiO_x/Ni solar cell structure. In PSC, despite a long diffusion length of charge carriers, a short circuit of the structure is very common in the presence of a small pinhole or nonuniformity in ETM compact layer or light absorber perovskite layer. In addition, reaching the metal back contact to the ETM layer (here the TiO_2 layer) leads to a considerable declination in V_{oc} and drop in cell performance. However, on the other side, there are some works that show a low performance decrease while electron and hole transport materials reach the surface contact. This phenomenon can be attributed to the wide gap between HOMO and LUMO levels of HTM and ETM, resulting in a drop in recombination rate as compared to transportation rate.[4,33] It is reported that, with infiltration mechanism of perovskite through FTO/compact TiO_2/mesoporous TiO_2/mesoporous NiO/carbon structure, the champion cell reaches 11.6% PCE with V_{oc} of 890 mV, current density of 18.2 mA/cm^2, and fill factor of 71%.[33] As discussed in the present study, because of large charge recombination resistance, contacting NiO and TiO_2 porous layers does not considerably deteriorate the cell performance. As shown in Figure 1d, in the case of a perovskite containing pinhole structure, the same structure of FTO/TiO_2/$CH_3NH_3PbI_{3-x}Cl_x$:NiO/Ni is developed. Thus, even if the perovskite could not completely cover the surface of the TiO_2 compact layer, using the engineered sputtering technique, NiO_x uniformly covers both perovskite and TiO_2 to inhibit short circuit of the cells, while depositing the Ni back contact. In this regard, a sandwiched perovskite with inorganic layers of compact TiO_2 and NiO_x is generated for better charge extraction. Hence, this method would be a comprehensive way of making a good junction between perovskite and NiO_x or the same electron blocking layers such as vanadium oxide (V_2O_5) and molybdenum trioxide (MoO_3) in the planar PSCs.

Figure 1e shows the grown rutile phase of TiO_2 with corresponding JCPDS card 21-1276 on the FTO substrate.

Although deposition of perovskite layers by chemical methods is very simple and cheap and creates coarse grain sizes consequently resulting in better performance in PSCs,[34] it mostly forms a nonuniform structure and contains pinholes. As shown in Figure 2a, deposition of the perovskite layer by the

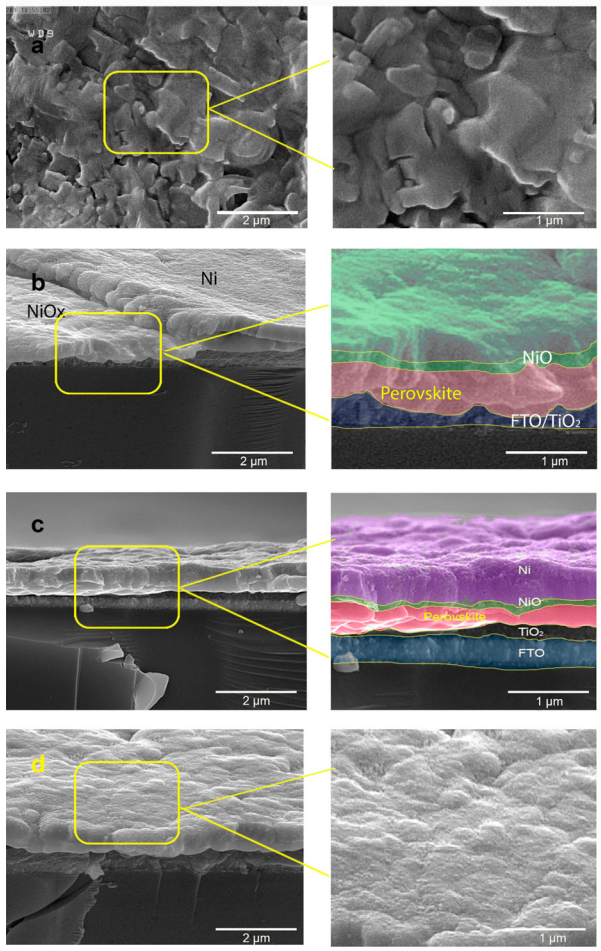

Figure 2. FE-SEM images of (a) perovskite layer on FTO/TiO_2 compact layer deposited at 2000 rpm and annealed for 100 °C, (b) cross sectional image of NiO_x layer on FTO/TiO_2/$CH_3NH_3PbI_{3-x}Cl_x$ by rotating 45° tilted substrate reactive magnetron sputtering, (c) cross sectional image of nickel contact layer on FTO/TiO_2/$CH_3NH_3PbI_{3-x}Cl_x$/NiO_x layer by nonrotating 90° substrate reactive magnetron sputtering. (d) The surface image of FTO/TiO_2/$CH_3NH_3PbI_{3-x}Cl_x$/NiO_x/Ni.

solution of $PbCl_2$ and CH_3NH_3I in DMF creates a rough, course-grain, and somehow nonuniform pinhole containing structure (perovskite synthesis and deposition procedures are described in Experimental Section). According to the direct-path deposition mechanism of sputtering, deposition of the NiO_x by rotating sputtering on this perovskite structure cannot cover the total surface of the perovskite and the pinholes (Figure S1a). As a result, there will be a weakness in surface coverage and compactness of NiO_x layer, leading to a major short circuit problem in the designed device. Surprisingly, by tilting the substrate for approximate 45° against the sputtering target, we could create a compact, pinhole-free, and uniform NiO_x layer on an almost whole surface of the perovskite and

DOI: 10.1021/acsami.5b05477
ACS Appl. Mater. Interfaces 2015, 7, 21807−21818

the possible existing pinholes in the perovskite layer, which previously caused the most major problem in a short circuit of the prepared cells (Figure 2b and Figure S1b). We used a nonrotating 90° deposition angle for depositing 250 nm of nickel contact on NiO_x electron blocking layer (Figure 2c and Figure S1c), relying on the compactness of NiO_x on the perovskite and pinholes, which creates a uniform NiO_x layer for landing the Ni atoms in back contact deposition. As shown in Figure 2d and Figure S2a,b, the final Ni contact layer uniformly covers the active area of the perovskite/NiO_x layer through a shadow mask.

During the sputtering, the plasma increases the substrate temperature because of high energy release during the hitting of nickel target by ionized oxygen and argon atoms. This procedure incredibly increases the substrate temperature in long deposition time and damages the perovskite layer, causing its degradation to PbI_2. Moreover, partial substrate temperature improves substrate adhesion to the perovskite layer and crystallinity of the NiO_x thin film. To control the substrate temperature during the sputtering, besides using cold-water circulation for cooling the target, we adjusted the distance between substrate and target and used periodic deposition with 15 min delay between every sequence. The maximum temperature rise in this work was 95 °C. Also, deposition sequences initiated after reaching the substrate temperature to 55 °C. As shown in the XRD pattern of Figure 3a and the photograph of back and top sides of the PSC (Figure S3), after several attempts, the modified deposited layers with 12 cm distances and 15 min delay between sequences showed no changes on the perovskite layers. The total deposition parameters are presented in the Supporting Information.

To investigate the surface topography changes and homogeneity, we used tapping and phase mode analyses of atomic force microscopy (AFM), respectively. Spatial maps of topography, phase image, and lineal roughness for surfaces of TiO_2/perovskite, perovskite/NiO_x, and perovskite/NiO_x/Ni are shown in Figure S4. As shown in Figure S4a,b, spin coating of the perovskite layer on TiO_2 layer shows some gross structures containing some pinholes. The nonhomogeneity of the perovskite layer is shown in the phase image of perovskite layer on TiO_2 (Figure S4c). According to XRD analysis, no PbI_2 phase was detected in the perovskite layer. Hence, the phase changes in the phase image can be attributed to surface phase changing from perovskite to TiO_2, implying the presence of pinholes in the perovskite structure. By deposition of surface containing perovskite and existing pinholes by 45° angular deposition of NiO_x, the surface showed more uniformity (Figures S4d,e) and complete homogeneity (Figure S4f). This behavior guarantees complete surface coverage by the NiO_x layer, and the absence of a pinhole to cause a short circuit in the final deposition of nickel back contact. In this study, the surface uniformity (Figures S4g,h) and homogeneity (Figure S4i) were improved by deposition of nickel back contact.

Although a majority of the PSCs prepared by organic HTM like spiro-OMeTAD show optimum performance in the first days of working, in this work we found the reverse behavior when using NiO_x as an HTM prepared by reactive magnetron sputtering. Figure 3b and Table 1 show the respective $J-V$ curves and parameters measured at AM1.5G solar illumination for inorganic sandwiched PSC at tracing of as-prepared samples and those after one, three, and six days. The as-prepared cells showed a low performance of 1.3%, with a V_{oc} magnitude of 0.69 V, current density of 3.09 mA/cm^2, and fill factor of 0.64.

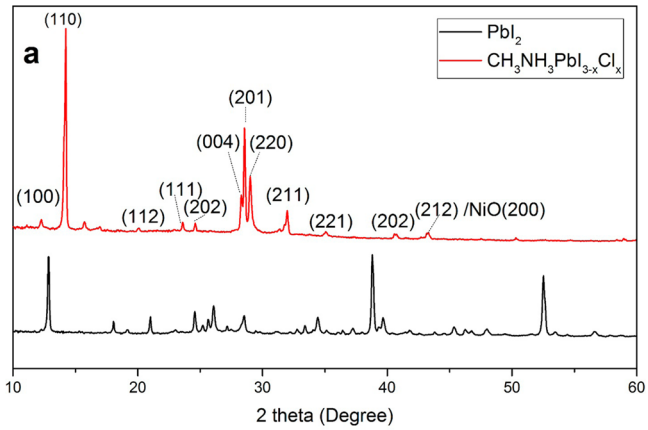

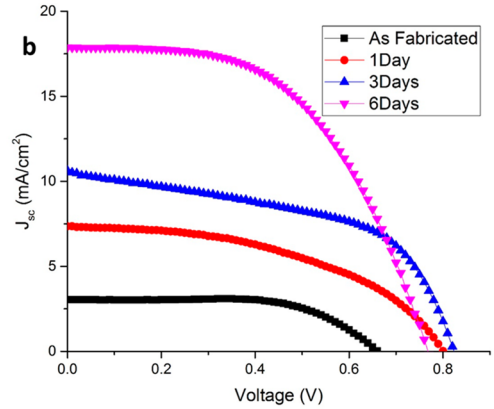

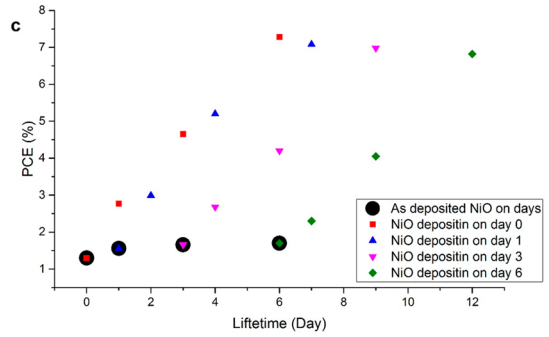

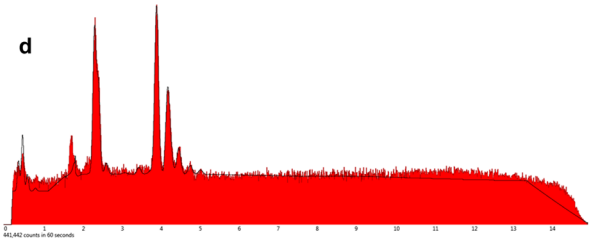

Element Number	Element Symbol	Element Name	Concentration
53	I	Iodine	49.0
82	Pb	Lead	22.4
7	N	Nitrogen	28.1
17	Cl	Chlorine	0.07

Figure 3. (a) XRD pattern of perovskite/NiO_x double layer and PbI_2 thin film. (b) $J-V$ curves measured at AM1.5G solar illumination for inorganic sandwiched perovskite solar cell of pristine sample and samples from one, three, and six days at tracing. (c) The device performance in various perovskite layer retention days of as-prepared sample and samples from one, three, and six days in the dry air followed by repeating the device analysis at lifetime days of one, three, and six. (d) EDS elemental analysis of deposited perovskite on the glass substrate.

DOI: 10.1021/acsami.5b05477
ACS Appl. Mater. Interfaces 2015, 7, 21807−21818

Table 1. Performance Parameters of the Sandwiched Inorganic Perovskite Solar Cell with 40 nm Nickel Oxide as a HTM at Tracing Days of As-Prepared Samples and Samples after One, Three, and Six Days

device lifetime (days)	V_{oc} (V)	J_{sc} (mA/cm^2)	FF	PCE (%)	NiO_x layer resistivity (Ω cm)
as-prepared	0.67	3.09	0.64	1.3	120
1	0.8	7.35	0.47	2.77	86
3	0.83	10.62	0.52	4.65	66
6	0.77	17.88	0.53	7.28	32

Unexpectedly, the day after, the cell performance increased to 2.77%, with a rise in both V_{oc} (0.8 V) and J_{sc} (7.35 mA/cm^2) and a drop in fill factor to 0.47. This improved cell performance can be attributed to declining resistivity of the NiO_x layer by decrease in residue strain developed during the sputtering process.[35] As reported before, annealing for a long time at low temperature or high temperature for a short time may release a large amount of residue strains generated during the sputtering method.[36,37] By releasing this strain in the interface of the perovskite and NiO_x layers, which is mostly posed to compressive strain at the low deposition pressure,[38] a good junction for charge transportation is potentially developed between perovskite and NiO_x layers. Thus, in addition to good charge transport leading to high current density, a charge recombination drop occurs in the interface of the perovskite and NiO_x layer and results in larger open circuit voltage. A decrease of the fill factor after 1 day can probably be explained by charge recombination within the NiO_x layer that still contains a large amount of defects.[39] On the third day, by increasing the cell parameters to V_{oc} of 0.83 V, current density of 10.62 mA/cm^2, and fill factor of 0.52, the cell performance reached 4.65%. As previously mentioned, both V_{oc} and current density are improved because of strain release and consequently high charge mobility in both interface and NiO_x layers. The fill factor in the third day increased possibly because of strain release in the NiO_x layer, which consequently results in low scattering charge effect and high hole mobility in the NiO_x layer.[40] On the sixth day, the perovskite cells showed the best performance of 7.28% with expected increase in fill factor and current density. As shown in Figure 3b and Table 1, the open circuit of the cell drops to 0.77 V, probably due to the high charge transport induced from an approximate strain release in a 40 nm thick NiO_x layer both in the interface and the NiO_x layer. This drip implies that high charge transport does not allow high charge accumulation at the Fermi level, which consequently causes a lower state of the Fermi level and lower V_{oc}. By day six, since the deposited layer of NiO_x on perovskite layer results in no change in the final surface coverage, the high rise of current density to 17.88 mA/cm^2 could be because of decreasing NiO_x resistivity and high charge extraction capability by the NiO_x layer. Besides, as both electronic properties and surface coverage of perovskite by NiO_x layers play a key role in emerging high current density in PSCs, it is implied that a good coverage of the perovskite layer by the NiO_x layer is obtained in this work. Through this coverage, the cell could reach a high

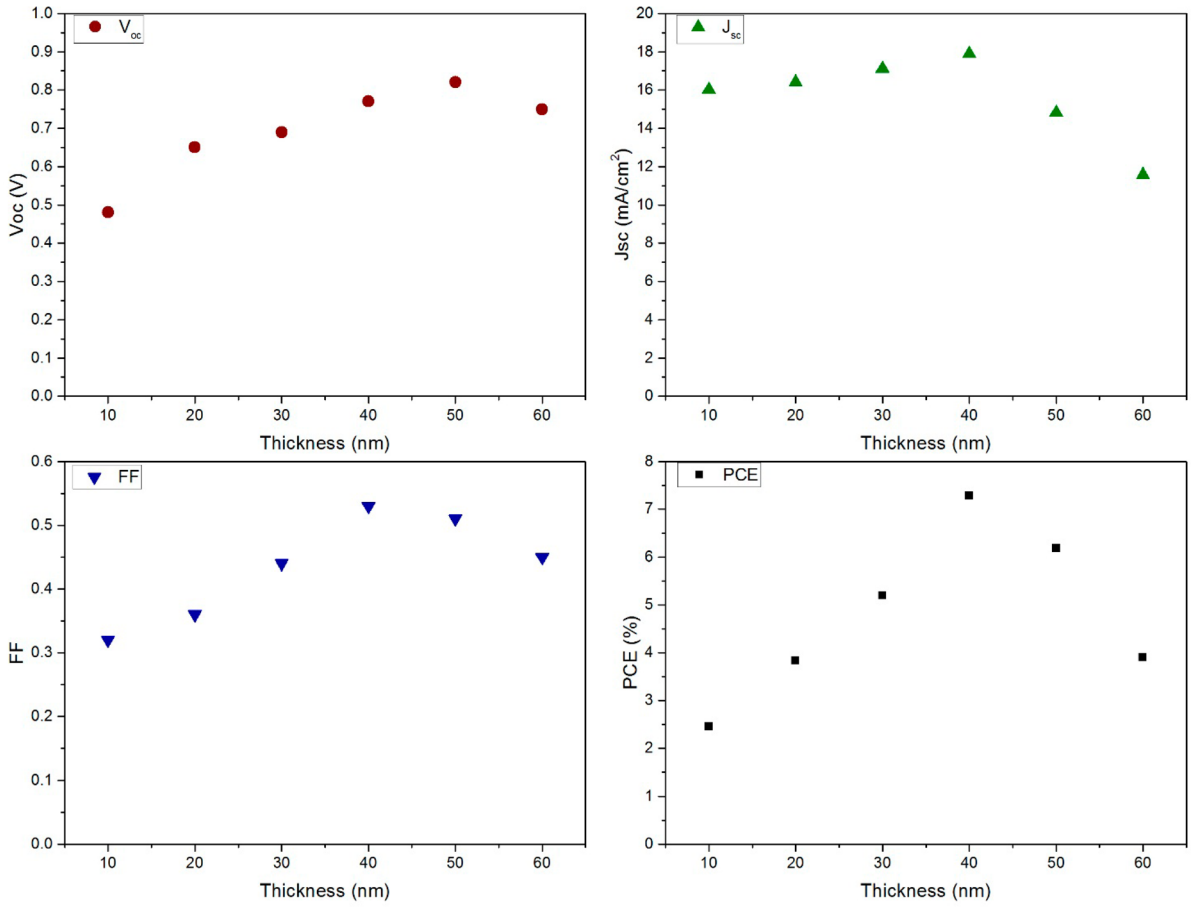

Figure 4. Thickness dependence of NiO_x electron blocking layer on device performance parameters.

DOI: 10.1021/acsami.5b05477
ACS Appl. Mater. Interfaces 2015, 7, 21807−21818

current density by benefiting from high charge extraction properties of the TiO_2 and NiO_x layer. The same behavior was observed with some deterioration in performance by annealing of the device at 70 °C up to 12 h, rather than long-term room temperature annealing. This behavior is explained by structure grossing and formation of some defects in the interfaces of NiO_x and perovskite layers through fast annealing process. So, the time necessity can be facilitated and simulated with annealing temperature. We performed the resistivity measurement of the NiO_x layer at the device lifetime of as-prepared, day one, day three, and day six to study the resistivity change over six days. A four-point collinear probe method was used to measure the sheet resistivity. As shown in Table 1, the resistivity of the sheet decreased by day six. The drop of sheet resistivity of sputtered NiO_x, which can result from increasing the carrier mobility by releasing the sheet resistance in 6 days or 12 h annealing at 70 °C, causes an improvement in the cell performance up to 4.6 times that of the as-prepared cells. Furthermore, as reported before, deposition of the NiO_x layer at low temperature generates greater carrier concentration which causes lower resistivity.[41]

To study the comparative enhancement of the device by intrinsic perovskite and NiO_x layer enhancement from six days of working, after deposition of the perovskite layer we kept the perovskite layers in dry air (80% pure nitrogen and 20% pure oxygen) followed by deposition of the NiO_x layer at various retaining days of one, three, and six. The deposited NiO_x layer was kept in and analyzed at the same device lifetime of one, three, and six days after deposition. As shown in Figure 3c, deposition of NiO_x on the perovskite layers retained in the dry air indicates just a slight increase within the first day of retention with no considerable change in further retention days of 3 and 6. Thus, it can be concluded that device enhancement by the perovskite structure is negligible as compared to that of strain release of the NiO_x layer by six days. Further tracing of the prepared devices at various retention times showed a similar increment in device performance at the cell lifetime of as-prepared samples and those after one, three, and six days

To reveal the value of the Cl in the structure, we performed EDS characterization analysis to estimate the existence of chlorine in the structure. As shown in Figure 3d, the detected amount of chlorine by EDS measurement was around 0.07% that is negligible compared to the 49% of iodine in the perovskite structure. Hence, the chlorine might never contribute in the perovskite structure, so that the present perovskite structure could be $CH_3NH_3PbI_3$. Therefore, by forming the perovskite layer from respective 1:3 ratio of $PbCl_2$:CH_3NH_3I in DMF, the probable structure of perovskite would be $CH_3NH_3PbI_3$. Note that the same behavior was previously proposed by Wai Ng[42] and Gratzel.[43]

To study the effect of NiO_x thickness on cell performance parameters, various NiO_x thin film thicknesses of 10, 20, 30, 40, 50, and 60 nm were deposited on the perovskite layer under the same deposition condition. The characterized cell parameters shown in Figure 4 indicate that, with no NiO_x deposition, a serious short circuit is created due to the large amount of pinholes existing in perovskite structure. Increasing the NiO_x thickness from 10 nm may decrease the probability of surface coverage defects. Accordingly, as shown in Figure 4a, the magnitude of V_{oc} drops as the thickness of the NiO_x thin film decreases. The increase in thickness of the NiO_x layer does not affect the current density of the cell until it exceeds 40 nm, so that there probably might be no considerable change in NiO_x thin film resistivity up to thickness of 40 nm. However, once this thickness exceeds 40 nm, the resistivity of the NiO_x layer increases and causes a noticeable charge transport limitation. Fill factor of the cells showed somehow the same behavior of an open circuit for various NiO_x thicknesses. Since the major decrease in fill factor could be attributed to charge recombination of interface and transport materials, a slight decrease in fill factor for 50 nm was observed, where this drop can be explained by the charge recombination induced by transport resistance and produced traps in high NiO_x layer thicknesses.[44] At higher NiO_x thickness of 60 nm, the cell parameters continued deteriorating, and cell performance considerably weakened.

The durability of the cells was traced by keeping the fabricated cells at 25 °C ambient atmosphere with 28 ± 2% moisture, in comparison to similar structure fabricated with spiro-OMeTAD and silver as a standard sample. As shown in Figure 5, the fabricated perovskite cell with NiO_x as an HTM

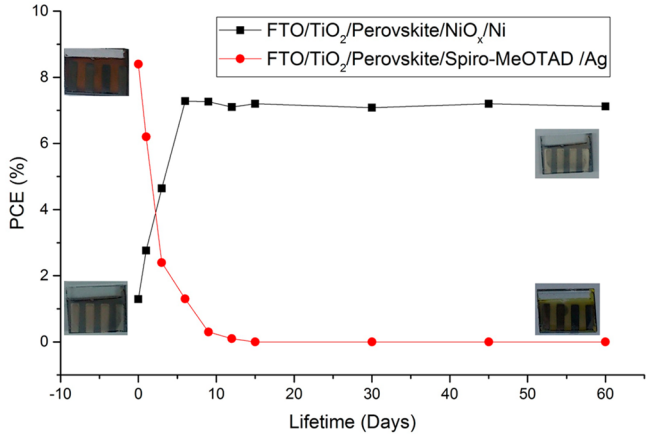

Figure 5. Device performance durability of top side of FTO/TiO_2/$CH_3NH_3PbI_{3-x}Cl_x$/NiO_x/Ni and back side of FTO/TiO_2/$CH_3NH_3PbI_{3-x}Cl_x$/spiro-OMeTAD/Ag by 60 days.

reaches maximum efficiency of 7.24% after 6 days and remains approximately stable for 60 days. On the other hand, the same structure with spiro-OMeTAD as an HTM started deteriorating just after having a maximum efficiency of 8.24% at the first stage of fabrication and was completely out of efficiency by 12 days. The HTM layer as the outermost layer, despite having a good hole extraction affinity, could play as a surface shield for water and oxygen diffusion barrier. The HTM layer properties such as density, uniformity, hydrophobicity, and vulnerable reactivity with water can affect the cell durability. As shown in Figure 5, spiro-OMeTAD cannot protect the perovskite from degradation, while NiO_x remains stable even after 2 months. As widely reported, deposition of NiO_x by reactive sputtering shows a compact and very dense layer through which there is a low chance for water molecules to diffuse. Note that, in addition to intrinsic strong physical properties of the inorganic NiO_x layer, deposition of inorganic semiconductors by sputtering shows strong surface mechanical properties such as scratching, indentation, and wear resistance.[45,46] Hence, the finished surface, as well as high capsulation properties of deposited NiO_x layer on perovskite, can protect the perovskite layer against mechanical damage.

Optical properties of single and multilayer PSCs were studied by UV−vis spectroscopy using two precise optical channels of

DOI: 10.1021/acsami.5b05477
ACS Appl. Mater. Interfaces 2015, 7, 21807−21818

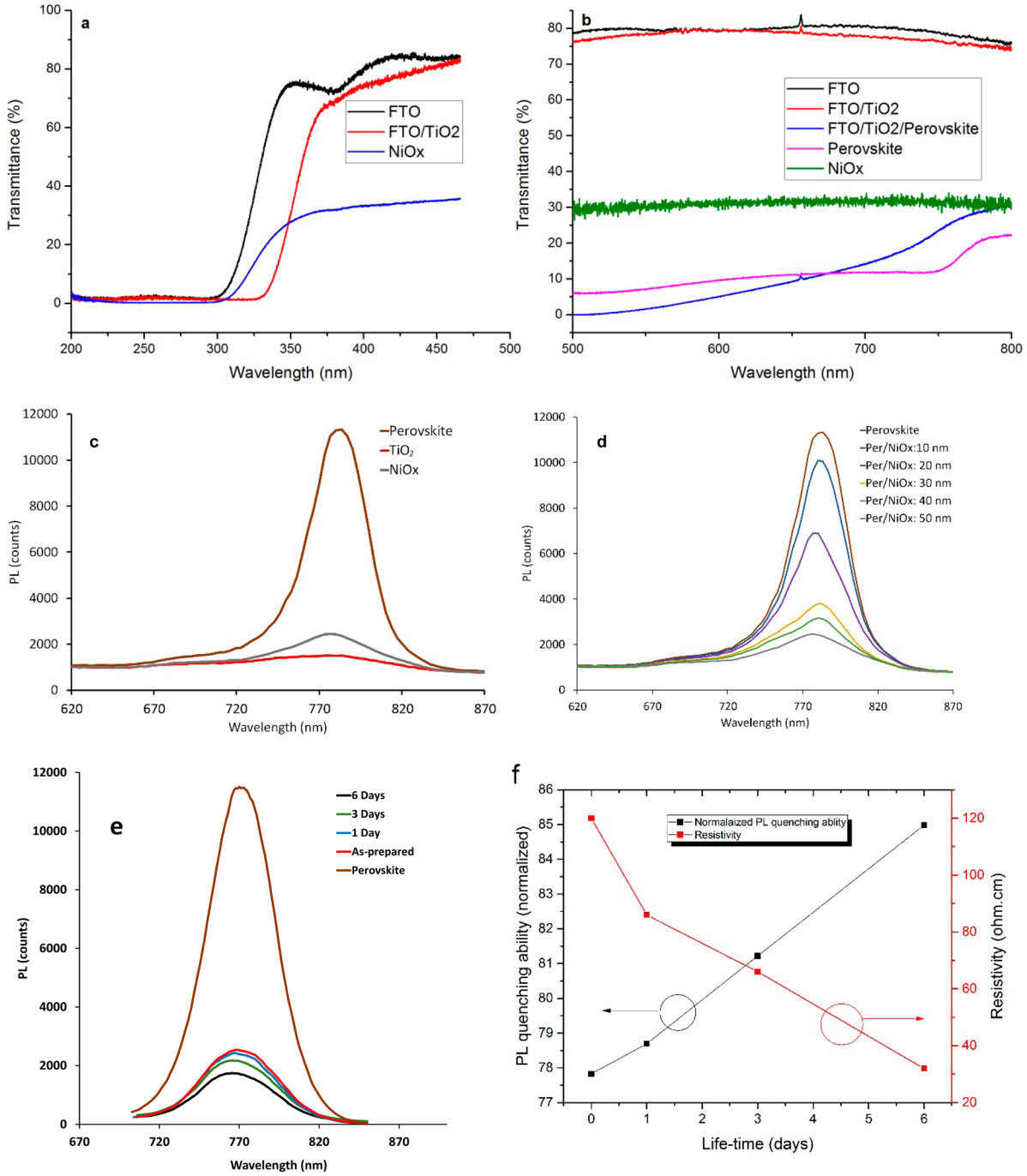

Figure 6. (a, b) Transmittance spectra of layers. (c) Perovskite photoluminescence study of single and double layers by 600 nm wavelength excitation for electron and hole transport materials of a sandwiched perovskite solar cell. (d) Various NiO_x thickness effect on perovskite photoluminescence spectra. (e) NiO_x/perovskite lifetime effects on perovskite photoluminescence spectra. (f) NiO_x layer resistivity and NiO_x/perovskite photoluminescence quenching ability in different lifetimes of the device. The normalized value of photoluminescence quenching ability was defined by the ratio of the photoluminescence value of the perovskite/NiO_x double layer at different lifetimes of as-prepared samples and those after one, three, and six days to the pure value of the single perovskite layer.

200−500 nm and 500−900 nm (Figure 6). Since perovskite layers indicated an absorbing ranging from 500 to 800 nm, a 500−900 nm channel was applied in this work to investigate optical properties of perovskite layers. As shown in Figure 6a, there is a slight shift in absorbing edge to larger wavelength by coating the TiO_2 thin layer on FTO. In addition, there is no obvious transmittance below 350 nm, so the whole wavelength lower than 350 nm is diminished by FTO and TiO_2 layers. The figure also indicates that there is a larger band gap for NiO_x around 3.6 eV which confirms a wide enough band gap for NiO_x as an HTM. Figure 6b presents visible spectroscopy of FTO, FTO/TiO_2, FTO/TiO_2/perovskite, glass/perovskite, and glass/NiO layers. This spectroscopy for FTO and FTO/TiO_2 shows large transmittance, so that a big share of light intensity is absorbed by the perovskite layer. Moreover, since the NiO_x layer is the upper layer of perovskite, its low transmittance does not affect the cell performance. The figure also shows an alteration in absorbance of FTO/TiO_2/perovskite and glass/

DOI: 10.1021/acsami.5b05477
ACS Appl. Mater. Interfaces 2015, 7, 21807−21818

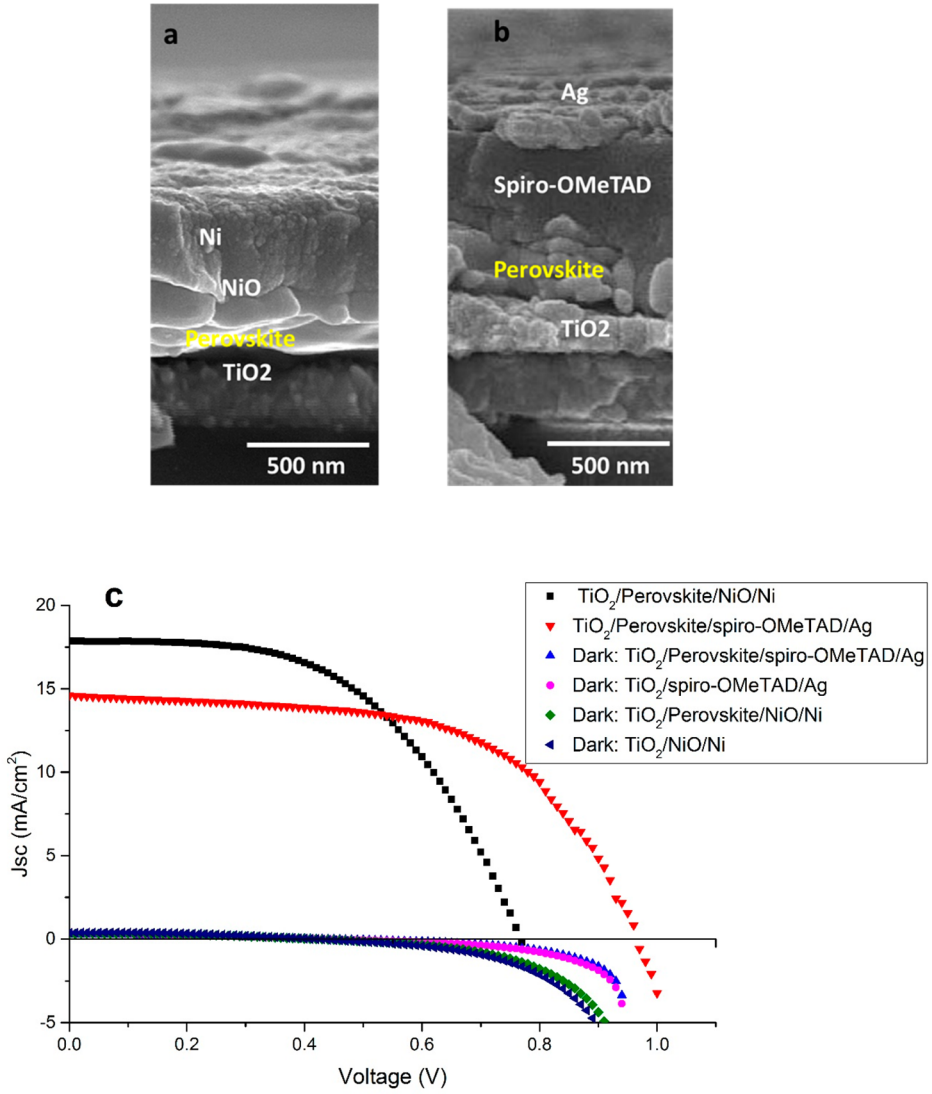

Figure 7. (a and b) FE-SEM images and (c) $J-V$ curves of FTO/TiO_2/$CH_3NH_3PbI_{3-x}Cl_x$/NiO_x/Ni and representative FTO/TiO_2/$CH_3NH_3PbI_{3-x}Cl_x$/spiro-MeOTAD/Ag under light and dark with and without the perovskite layer.

perovskite layers at 680 nm probably because of the surface morphology of perovskite layers that induces various scattering properties. Thus, deposition of the perovskite layer on TiO_2 substrate created by chemical bath deposition produces different morphologies than those of perovskite layer on the glass substrate. It is worth mentioning that the deposited perovskite layer on the TiO_2 layer shows a dark brown color, whereas deposition of perovskite on glass produces a dark black color.

To study the charge extraction properties of double layers, we studied the PL quenching properties of double layers. The PL of perovskite, perovskite/NiO_x, TiO_2/perovskite, and perovskite/(various thickness of NiO_x) on glass substrate was measured. The 600 nm excitation light was irradiated from the opposite side of the quenching layer with an incidental angle of 30°, and the photoluminescence was collected (Figure 6a,b). As shown in Figure 6a, TiO_2 as an electron transport layer could quench the photoluminescence of the perovskite layer by a high rate electron extraction from perovskite layer. Besides, for its considerable hole extraction ability obtained from the perovskite layer, NiO_x can be a good candidate for hole extraction and transportation materials. Investigation of various NiO_x thicknesses on hole extraction ability were also conducted using the photoluminescence spectra from glass/perovskite/NiO_x (10−50 nm) layers. Increasing the NiO_x thickness by 40 nm can significantly quench the photoluminescence of perovskite probably due to a drop in thin film resistivity, while increasing the thickness to 50 nm decreases the hole extraction ability of NiO_x layer possibly due to a larger amount of defects and low carrier concentration in thicker layers. We performed PL study of the perovskite/NiO_x double layer at the working times of as-prepared samples and those after one, three, and six days. Figure 6e shows gradual increase in quenching ability of holes by NiO_x layer by 6 days. As shown in Figure 6f, by decreasing the sheet resistivity by 6 days, which might be caused by strain releasing of the NiO_x layer in both the interface and the NiO_x layer, the charge extraction ability of the NiO_x increased and, in turn, resulted in a drop in the recombination resistance in the interface of NiO_x and perovskite layers.

As well as durability, we studied and compared the performance of the perovskite layers with two different HTM/contact couples of spiro-OMeTAD/Ag and NiO_x/Ni. As shown in Figure 7, the cells prepared with NiO_x/Ni as a

DOI: 10.1021/acsami.5b05477
ACS Appl. Mater. Interfaces 2015, 7, 21807−21818

HTM/contact layer indicate an efficiency value just 1% less than that of the same structure prepared by spiro-OMeTAD/Ag as an HTM/contact layer. The prepared cells with NiO_x show larger current density as compared to that of the same cell prepared by spiro-OMeTAD. This behavior can be probably ascribed to the good junction at the interface and good charge extraction properties of the NiO_x layer. The lower magnitude of V_{oc} in the FTO/TiO_2/perovskite/NiO_x/Ni device than the same structure of FTO/TiO_2/perovskite/spiro-OMeTAD/Ag may be due to higher recombination in the interface of NiO_x and TiO_2. Therefore, cell performance can be improved by increasing the V_{oc} and fill factor, once the pinholes in the perovskite are removed. We performed the dark $J-V$ analysis to study the recombination resistance of the prepared perovskite solar cells prepared by NiO and spiro-OMeTAD as HTM. In addition, to present the pinholed perovskite effect, the prepared cells with and without perovskite layers were investigated. As shown in Figure 7c, despite the high charge recombination resistance in the NiO and TiO_2 interface, this interface shows lower recombination resistance in comparison to the same architecture prepared by spiro-OMeTAD as an HTM. As shown in Figure 7c, the existence of pinholed perovskite layer between NiO and TiO_2 or spiro-OMeTAD and TiO_2 layers did not considerably affect the dark $J-V$ results and current density of the cells, probably due to large number of pinholes in the perovskite layer.

4. CONCLUSION

In summary, we introduced a successful technique of physical deposition of NiO_x as an HTM on the perovskite layer for strong charge extraction. In this paper, we depicted whole inorganic sandwiched PSC with an efficient champion PCE of 7.28%. Use of a new reactive magnetron sputtering technique was discussed for gaining good coverage and junction between perovskite and NiO_x layer at low deposition temperature. According to sputtering deposition method for NiO_x described in the main text, this technique can be used for other perovskite deposition procedures, resulting in various perovskite structures even with pinholes. Upon removal of NiO_x thin film strain by time passing (long time room temperature annealing), the cell performance enhances from 1.3% to 7.28%. The prepared cells showed an interesting long-term durability over more than 2 months, while the performance of the same structure with spiro-OMeTAD as HTM and silver as back contact quickly declined within the first days of working and completely deteriorated by 12 days. In addition to valuable cell performance and long-term durability, the preparation cost of the cell with the FTO/TiO_2/$CH_3NH_3PbI_{3-x}Cl_x$/NiO_x/Ni structure is quite low compared to that of the FTO/TiO_2/$CH_3NH_3PbI_{3-x}Cl_x$/spiro-OMeTAD/Ag structure. Hence, this structure has great potential to hit the PSC market.

■ ASSOCIATED CONTENT

Supporting Information

The Supporting Information is available free of charge on the ACS Publications website at DOI: 10.1021/acsami.5b05477.

Deposition schematic of NiO_x and Ni by dc reactive magnetron sputtering, FE-SEM image of perovskite layer and deposited NiO_x layer, photograph of back and top sides of device, and tapping and phase analysis mode of AFM images (PDF)

■ AUTHOR INFORMATION

Corresponding Author

*Phone/fax: 0098 21 82883368. E-mail: v_ahmadi@modares.ac.ir.

Notes

The authors declare no competing financial interest.

■ ACKNOWLEDGMENTS

The authors acknowledge financial support from Tarbiat Modares University and the equipment services from NOPL laboratory. The authors thank Dr. M. Eskandari and Ms. A. Khazaeipour for technical assistant at NOPL laboratory.

■ ABBREVIATIONS

HTM, hole transport material
ETM, electron transport material
spiro-OMeTAD, 2,2′,7,7′-tetrakis (*N*,*N*-di-*p*-methoxyphenyl-amine)-9,9′-spirobifluorene
PCE, power conversion efficiency
J_{sc}, short-circuit current density
FF, fill factor
V_{oc}, open circuit voltages
PL, photoluminescence
PEDOT:PSS, poly(3,4-ethylenedioxythiophene)
P3HT, poly(3-hexylthiophene)
PTAA, poly[bis(4-phenyl)(2,4,6-trimethylphenyl)amine]
CNT, carbon nanotube
PCBM, [6,6]-phenyl-C61-butyric acid methyl ester
HOMO, highest occupied molecular orbital
LUMO, lowest unoccupied molecular orbital

■ REFERENCES

(1) Snaith, H. J. Perovskites: The Emergence of a New Era for Low-Cost, High-Efficiency Solar Cells. *J. Phys. Chem. Lett.* **2013**, *4* (21), 3623−3630.

(2) Park, N.-G. Organometal Perovskite Light Absorbers Toward a 20% Efficiency Low-Cost Solid-State Mesoscopic Solar Cell. *J. Phys. Chem. Lett.* **2013**, *4* (15), 2423−2429.

(3) Chiang, Y.-F.; Jeng, J.-Y.; Lee, M.-H.; Peng, S.-R.; Chen, P.; Guo, T.-F.; Wen, T.-C.; Hsu, Y.-J.; Hsu, C.-M. High Voltage and Efficient Bilayer Heterojunction Solar Cells Based on an Organic-inorganic Hybrid Perovskite Absorber With a Low-cost Flexible Substrate. *Phys. Chem. Chem. Phys.* **2014**, *16* (13), 6033−6040.

(4) Kim, H.-S.; Lee, C.-R.; Im, J.-H.; Lee, K.-B.; Moehl, T.; Marchioro, A.; Moon, S.-J.; Humphry-Baker, R.; Yum, J.-H.; Moser, J. E.; Gratzel, M.; Park, N.-G. Lead Iodide Perovskite Sensitized All-Solid-State Submicron Thin Film Mesoscopic Solar Cell with Efficiency Exceeding 9%. *Sci. Rep.* **2012**, *2*, 591.

(5) Stranks, S. D.; Eperon, G. E.; Grancini, G.; Menelaou, C.; Alcocer, M. J. P.; Leijtens, T.; Herz, L. M.; Petrozza, A.; Snaith, H. J. Electron-Hole Diffusion Lengths Exceeding 1 Micrometer in an Organometal Trihalide Perovskite Absorber. *Science* **2013**, *342* (6156), 341−344.

(6) Im, J.-H.; Lee, C.-R.; Lee, J.-W.; Park, S.-W.; Park, N.-G. 6.5% Efficient Perovskite Quantum-dot-sensitized Solar Cell. *Nanoscale* **2011**, *3* (10), 4088−4093.

(7) Xing, G.; Mathews, N.; Sun, S.; Lim, S. S.; Lam, Y. M.; Grätzel, M.; Mhaisalkar, S.; Sum, T. C. Long-Range Balanced Electron- and Hole-Transport Lengths in Organic-Inorganic CH3NH3PbI3. *Science* **2013**, *342* (6156), 344−347.

(8) Zhou, H.; Chen, Q.; Li, G.; Luo, S.; Song, T.-b.; Duan, H.-S.; Hong, Z.; You, J.; Liu, Y.; Yang, Y. Interface Engineering of Highly Efficient Perovskite Solar Cells. *Science* **2014**, *345* (6196), 542−546.

(9) http://www.nrel.gov/ncpv/images/efficiency_chart.jpg.

DOI: 10.1021/acsami.5b05477
ACS Appl. Mater. Interfaces 2015, 7, 21807−21818

(10) Kumar, M. H.; Yantara, N.; Dharani, S.; Graetzel, M.; Mhaisalkar, S.; Boix, P. P.; Mathews, N. Flexible, Low-temperature, Solution Processed ZnO-based Perovskite Solid State Solar Cells. *Chem. Commun.* **2013**, *49* (94), 11089−11091.
(11) Im, J.-H.; Jang, I.-H.; Pellet, N.; Grätzel, M.; Park, N.-G. Growth of $CH_3NH_3PbI_3$ Cuboids With Controlled Size for High-efficiency Perovskite Solar Cells. *Nat. Nanotechnol.* **2014**, *9* (11), 927−932.
(12) Docampo, P.; Ball, J. M.; Darwich, M.; Eperon, G. E.; Snaith, H. J. Efficient Organometal Trihalide Perovskite Planar-heterojunction Solar Cells on Flexible Polymer Substrates. *Nat. Commun.* **2013**, *4*, 2761.
(13) You, J.; Hong, Z.; Yang, Y.; Chen, Q.; Cai, M.; Song, T.-B.; Chen, C.-C.; Lu, S.; Liu, Y.; Zhou, H. Low-Temperature Solution-Processed Perovskite Solar Cells with High Efficiency and Flexibility. *ACS Nano* **2014**, *8* (2), 1674−1680.
(14) Roldan-Carmona, C.; Malinkiewicz, O.; Soriano, A.; Minguez Espallargas, G.; Garcia, A.; Reinecke, P.; Kroyer, T.; Dar, M. I.; Nazeeruddin, M. K.; Bolink, H. J. Flexible High Efficiency Perovskite Solar Cells. Energy Environ. *Energy Environ. Sci.* **2014**, *7* (3), 994−997.
(15) Habisreutinger, S. N.; Leijtens, T.; Eperon, G. E.; Stranks, S. D.; Nicholas, R. J.; Snaith, H. J. Carbon Nanotube/Polymer Composites as a Highly Stable Hole Collection Layer in Perovskite Solar Cells. *Nano Lett.* **2014**, *14* (10), 5561−5568.
(16) Li, Z.; Kulkarni, S. A.; Boix, P. P.; Shi, E.; Cao, A.; Fu, K.; Batabyal, S. K.; Zhang, J.; Xiong, Q.; Wong, L. H.; Mathews, N.; Mhaisalkar, S. G. Laminated Carbon Nanotube Networks for Metal Electrode-Free Efficient Perovskite Solar Cells. *ACS Nano* **2014**, *8* (7), 6797−6804.
(17) Jeng, J.-Y.; Chiang, Y.-F.; Lee, M.-H.; Peng, S.-R.; Guo, T.-F.; Chen, P.; Wen, T.-C. CH3NH3PbI3 Perovskite/Fullerene Planar-Heterojunction Hybrid Solar Cells. *Adv. Mater.* **2013**, *25* (27), 3727−3732.
(18) Wang, K.-C.; Jeng, J.-Y.; Shen, P.-S.; Chang, Y.-C.; Diau, E. W.-G.; Tsai, C.-H.; Chao, T.-Y.; Hsu, H.-C.; Lin, P.-Y.; Chen, P.; Guo, T.-F.; Wen, T.-C. p-type Mesoscopic Nickel Oxide/Organometallic Perovskite Heterojunction Solar Cells. *Sci. Rep.* **2014**, *4*, 4756.
(19) Mei, A.; Li, X.; Liu, L.; Ku, Z.; Liu, T.; Rong, Y.; Xu, M.; Hu, M.; Chen, J.; Yang, Y.; Grätzel, M.; Han, H. A Hole-conductor−free, Fully Printable Mesoscopic Perovskite Solar Cell With High Stability. *Science* **2014**, *345* (6194), 295−298.
(20) Zhang, L.; Liu, T.; Liu, L.; Hu, M.; Yang, Y.; Mei, A.; Han, H. The Effect of Carbon Counter Electrodes on Fully Printable Mesoscopic Perovskite Solar Cells. *J. Mater. Chem. A* **2015**, *3* (17), 9165−9170.
(21) Kim, H.-S.; Lee, J.-W.; Yantara, N.; Boix, P. P.; Kulkarni, S. A.; Mhaisalkar, S.; Grätzel, M.; Park, N.-G. High Efficiency Solid-State Sensitized Solar Cell-Based on Submicrometer Rutile TiO_2 Nanorod and CH3NH3PbI3 Perovskite Sensitizer. *Nano Lett.* **2013**, *13* (6), 2412−2417.
(22) Cai, B.; Xing, Y.; Yang, Z.; Zhang, W.-H.; Qiu, J. High Performance Hybrid Solar Cells Sensitized By Organolead Halide Perovskites. *Energy Environ. Sci.* **2013**, *6* (5), 1480−1485.
(23) Liu, D.; Kelly, T. L. Perovskite Solar Cells With a Planar Heterojunction Structure Prepared Using Room-temperature Solution Processing Techniques. *Nat. Photonics* **2014**, *8* (2), 133−138.
(24) Lee, M. M.; Teuscher, J.; Miyasaka, T.; Murakami, T. N.; Snaith, H. J. Efficient Hybrid Solar Cells Based on Meso-Superstructured Organometal Halide Perovskites. *Science* **2012**, *338* (6107), 643−647.
(25) Edri, E.; Kirmayer, S.; Cahen, D.; Hodes, G. High Open-Circuit Voltage Solar Cells Based on Organic−Inorganic Lead Bromide Perovskite. *J. Phys. Chem. Lett.* **2013**, *4* (6), 897−902.
(26) Christians, J. A.; Fung, R. C. M.; Kamat, P. V. An Inorganic Hole Conductor for Organo-Lead Halide Perovskite Solar Cells. Improved Hole Conductivity with Copper Iodide. *J. Am. Chem. Soc.* **2014**, *136* (2), 758−764.
(27) Qin, P.; Tanaka, S.; Ito, S.; Tetreault, N.; Manabe, K.; Nishino, H.; Nazeeruddin, M. K.; Grätzel, M. Inorganic Hole Conductor-based Lead Halide Perovskite Solar Cells With 12.4% Conversion Efficiency. *Nat. Commun.* **2014**, *5*, 3834.
(28) Zhu, Z.; Bai, Y.; Zhang, T.; Liu, Z.; Long, X.; Wei, Z.; Wang, Z.; Zhang, L.; Wang, J.; Yan, F.; Yang, S. High-Performance Hole-Extraction Layer of Sol−Gel-Processed NiO Nanocrystals for Inverted Planar Perovskite Solar Cells. *Angew. Chem., Int. Ed.* **2014**, *53* (46), 12571−12575.
(29) Jiang, Q.; Sheng, X.; Shi, B.; Feng, X.; Xu, T. Nickel-Cathoded Perovskite Solar Cells. *J. Phys. Chem. C* **2014**, *118* (45), 25878−25883.
(30) Liu, M.; Johnston, M. B.; Snaith, H. J. Efficient Planar Heterojunction Perovskite Solar Cells By Vapour Deposition. *Nature* **2013**, *501* (7467), 395−398.
(31) Yella, A.; Heiniger, L.-P.; Gao, P.; Nazeeruddin, M. K.; Grätzel, M. Nanocrystalline Rutile Electron Extraction Layer Enables Low-Temperature Solution Processed Perovskite Photovoltaics with 13.7% Efficiency. *Nano Lett.* **2014**, *14* (5), 2591−2596.
(32) Bi, D.; Moon, S.-J.; Haggman, L.; Boschloo, G.; Yang, L.; Johansson, E. M. J.; Nazeeruddin, M. K.; Gratzel, M.; Hagfeldt, A. Using a Two-step Deposition Technique to Prepare Perovskite ($CH_3NH_3PbI_3$) for Thin Film Solar Cells Based on ZrO_2 and TiO_2 Mesostructures. *RSC Adv.* **2013**, *3* (41), 18762−18766.
(33) Liu, Z.; Zhang, M.; Xu, X.; Bu, L.; Zhang, W.; Li, W.; Zhao, Z.; Wang, M.; Cheng, Y.-B.; He, H. P-Type Mesoscopic NiO as an Active Interfacial Layer for Carbon Counter Electrode Based Perovskite Solar Cells. *Dalton Trans.* **2015**, *44* (9), 3967−3973.
(34) Nie, W.; Tsai, H.; Asadpour, R.; Blancon, J.-C.; Neukirch, A. J.; Gupta, G.; Crochet, J. J.; Chhowalla, M.; Tretiak, S.; Alam, M. A.; Wang, H.-L.; Mohite, A. D. High-efficiency Solution-processed Perovskite Solar Cells With Millimeter-scale Grains. *Science* **2015**, *347* (6221), 522−525.
(35) Abdullahi, S.; Momoh, M.; Yahya, H. N. Influence of Nitrogen Annealing on the Structural and Electrical Properties of Zinc Oxide (ZnO) Tthin Film Deposited By Radio Frequency Magnetron Sputtering Technique. *IOSR J. Environ. Sci., Toxicol. Food Technol.* **2013**, *4* (4), 81−85.
(36) Chen, H.-L.; Lu, Y.-M.; Hwang, W.-S. Effect of Film Thickness on Structural and Electrical Properties of Sputter-Deposited Nickel Oxide Films. *Mater. Trans.* **2005**, *46* (4), 872−879.
(37) Kalpana, H. M.; Siddeswara Prasad, V.; Nayak, M. M. Influence of Annealing and Thickness on the Electrical Properties of Invar36 Thin Flm for Strain Gauge Applications. *Int. J. Thin Fil. Sci. Tec* **2013**, *2* (3), 155−161.
(38) Nejand, B. A.; Sanjabi, S.; Ahmadi, V. The Effect of Sputtering Gas Pressure on Structure and Photocatalytic Properties of Nano-structured Titanium Oxide Self-cleaning Thin Film. *Vacuum* **2010**, *85* (3), 400−405.
(39) Schuetze, A. P.; Lewis, W.; Brown, C.; Geerts, W. J. A Laboratory on the Four-point Probe Technique. *Am. J. Phys.* **2004**, *72* (2), 149−153.
(40) Janotti, A.; Van de Walle, C. G. Fundamentals of Zinc Oxide As a Semiconductor. *Rep. Prog. Phys.* **2009**, *72* (12), 126501.
(41) Fasaki, I.; Koutoulaki, A.; Kompitsas, M.; Charitidis, C. Structural, Electrical and Mechanical Properties of NiO Thin Films Grown By Pulsed Laser Deposition. *Appl. Surf. Sci.* **2010**, *257* (2), 429−433.
(42) Ng, T.-W.; Chan, C.-Y.; Lo, M.-F.; Guan, Z. Q.; Lee, C.-S. Formation Chemistry of Perovskites With Mixed Iodide/chloride Content and the Implications on Charge Transport Properties. *J. Mater. Chem. A* **2015**, *3* (17), 9081−9085.
(43) Dar, M. I.; Arora, N.; Gao, P.; Ahmad, S.; Grätzel, M.; Nazeeruddin, M. K. Investigation Regarding the Role of Chloride in Organic−Inorganic Halide Perovskites Obtained from Chloride Containing Precursors. *Nano Lett.* **2014**, *14* (12), 6991−6996.
(44) Wang, K.-C.; Shen, P.-S.; Li, M.-H.; Chen, S.; Lin, M.-W.; Chen, P.; Guo, T.-F. Low-Temperature Sputtered Nickel Oxide Compact Thin Film as Effective Electron Blocking Layer for Mesoscopic NiO/$CH_3NH_3PbI_3$ Perovskite Heterojunction Solar Cells. *ACS Appl. Mater. Interfaces* **2014**, *6* (15), 11851−11858.
(45) Venkatachalam, D. K.; Bradby, J. E.; Saleh, M. N.; Ruffell, S.; Elliman, R. G. Nanomechanical Properties of Sputter-deposited HfO_2 and $Hf_xSi_{1-x}O_2$ Thin Films. *J. Appl. Phys.* **2011**, *110* (4), 043527.

DOI: 10.1021/acsami.5b05477
ACS Appl. Mater. Interfaces 2015, 7, 21807−21818

(46) Khojier, K.; Savaloni, H.; Shokrai, E.; Dehghani, Z.; Dehnavi, N. Influence of Argon Gas Flow on Mechanical and Electrical Properties of Sputtered Titanium Nitride Thin Films. *J. Theor. Appl. Phys.* **2013**, *7* (1), 37.

DOI: 10.1021/acsami.5b05477
ACS Appl. Mater. Interfaces 2015, 7, 21807−21818